Supplementary Materials: Three-dimensional Near-field Analysis Through Peak Force Scattering-type Near-field Optical Microscopy

Haomin Wang[1], Jiahan Li[2], James H. Edgar[2], and Xiaoji G. Xu[1*]

[1]Department of Chemistry, Lehigh University, 6 E Packer Ave. Bethlehem, PA, 18015, USA

[2]Tim Taylor Department of Chemical Engineering, Kansas State University, Manhattan, Kansas 66506, USA

*Email: xgx214@lehigh.edu

Supplementary Note 1: Derivation of resonant conditions and calculation of fringe patterns

Resonant conditions of *h*-BN nano-disk resonators had been investigated thoroughly in the previous work.[1] According to it, the propagation of polaritons on the surface of *h*-BN micro-disk can also be described by a 2D wave equation:

$$(i\omega)^2\rho = v_p^2(\omega)\nabla^2\rho \tag{S1}$$

in which ρ is the spatial charge density, v_p is the phase velocity and ω is the angular frequency. Resonant conditions can be obtained by the standing wave solution of **Equation S1** using a Neumann boundary condition at the edge of disk with radius r_0, where we have:

$$\left.\frac{\partial\rho}{\partial r}\right|_{r=r_0} = 0 \tag{S2}$$

Solutions of the 2D wave equation are in forms of Bessel function with polar coordinate (r, θ):

$$\rho = J_s(kr)(A\cos(s\theta) + B\sin(s\theta))e^{i\omega t} \tag{S3}$$

in which J_s is the Bessel function of s^{th} order, k is the wave vector of polariton and A, B are arbitrary complex amplitudes. By solving **Equation S1** and **S2** together, one can get standing wave solutions that represents the resonant conditions of a circular disk:

$$\begin{gathered}\rho = J_s(k_{sn}r + \phi)(A\cos(s\theta) + B\sin(s\theta))e^{i\omega t} \\ \text{with } k_{sn} = n^{\text{th}} \text{ root of } J_s'(kr_0 + \phi) = 0\end{gathered} \tag{S4}$$

Note that a correction phase factor ϕ is added to account for the extra phase shift of polariton waves that have been reflected by the disk edge. In our case, we found $\phi = -0.28\pi$ best fit our experimental results, which agrees well with -0.28π [1] and -0.25π [2, 3] found in literatures.

Measuring ρ at different non-resonant and resonant conditions with an AFM tip and illumination light results to different signal contributions. The majority of PF-SNOM signal is from the so-called roundtrip component, which is circularly symmetric and independent of θ.[1] Thus, we can estimate PF-SNOM signal as roundtrip component:

$$\text{PF-SNOM signal} \propto \rho^2 = J_s^2(k_{sn}r + \phi) \tag{S5}$$

which can be used to calculate fringe patterns that we've seen in PF-SNOM images. Since the anomalous phase shift ϕ affects most the outermost fringe and cannot be easily accounted due to the presence of fringing field,[1] in our simulation of ρ^2 we omit this term to achieve optimal agreement between simulated fringes and PF-SNOM fringes.

Solving **Equation S4** gives out a series of k_{sn}, which should be relevant to experimentally observed resonant conditions. To assign a proper (s, n) pair to each resonant condition, we compare k_{sn} with q_{p} from FFT on PF-SNOM images at resonant conditions. The workflow is shown below:

1. Obtain resonant q_{p} from experimentally observed PF-SNOM images. In our case, we chose

PF-SNOM images at 1410, 1421, and 1428 cm^{-1} as three resonant conditions (since the momentum is locked no matter the change of tip-sample distance). Experimental fringe patterns at each resonant condition were extracted by performing a radial averaging from the disk center on each of resonant PF-SNOM image. Then, FFT was performed on each fringe pattern to get spatial frequency of the fringe k_{f}, which then was converted to the momentum of polariton q_{p} by $q_{\mathrm{p}} = \pi k_{\mathrm{f}}$.

2. A series of k_{sn} from solutions of **Equation S4** were plugged back into **Equation S5** to get simulated fringe patterns ρ^2.
3. Compare k_{sn} with q_{p} and ρ^2 with experimental fringe patterns. If they match, assign corresponding mode numbers (s, n) to this resonant frequency.

Parameters that are used in these steps for resonant conditions shown in the main text **Figs. 2e-f** are summarized in **Table S1**, from which we found that the resonances that we observed by PF-SNOM mainly correspond to modes with $s = 0$ or 1. $s = 0$ corresponds to modes that show the maximal signal at disk center, while $s = 1$ corresponds to modes that show the minimal at disk center (**Supplementary Fig. S5**).

Table S1 Parameters used in the assignment of (s, n)

Resonant frequencies (cm^{-1})	q_{p} (μm^{-1})	(s, n)	k_{sn} (μm^{-1})	Parameters used in solving **Eq. S4**
1410	2.11	(1,3)	2.08	$\phi = -0.28\pi$ $r_0 = 4.5\ \mu m$
1421	2.48	(0,4)	2.44	
1428	2.84	(1,4)	2.78	

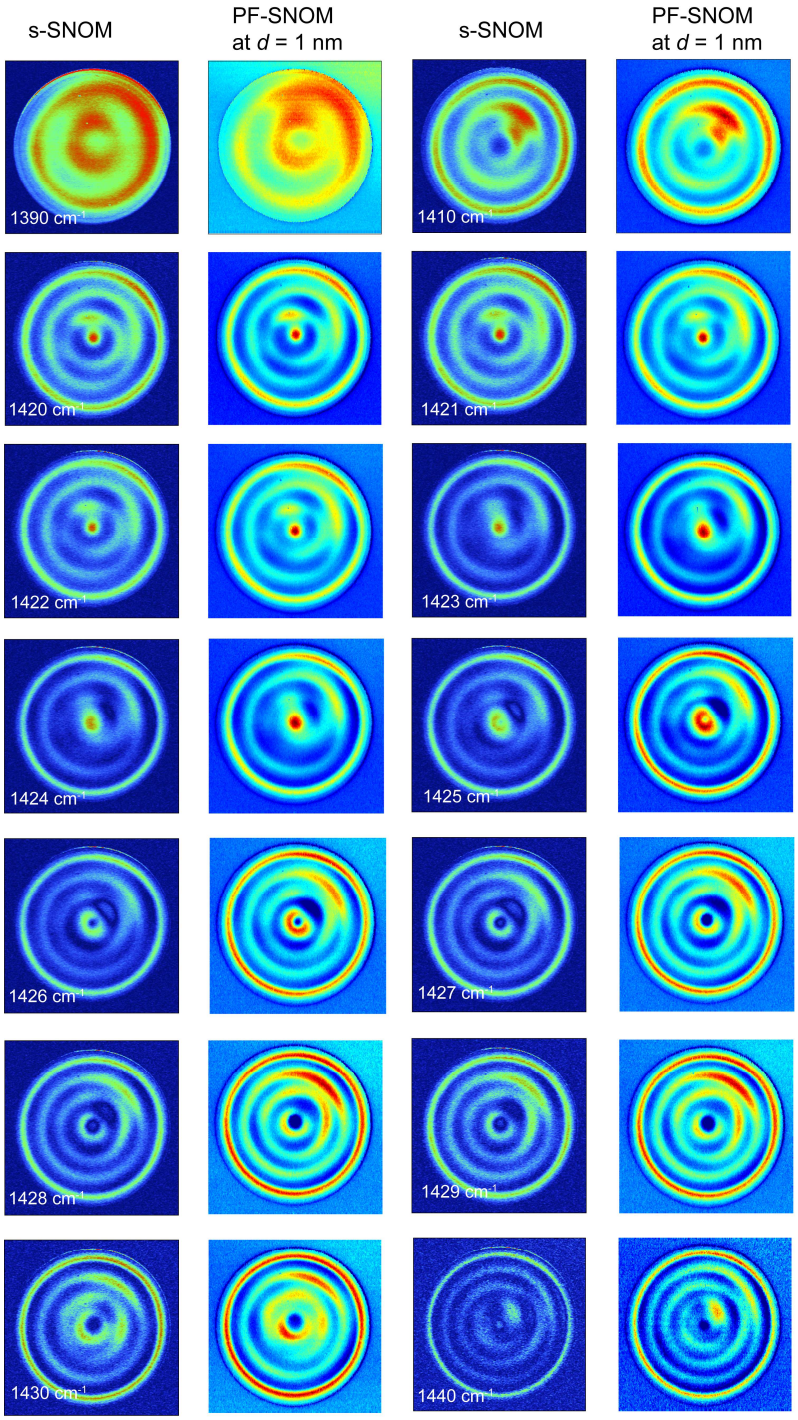

Supplementary Figure S1. s-SNOM and PF-SNOM images. s-SNOM images are obtained using the same homodyne setup as PF-SNOM. The AFM tip is mechanically driven by a piezo at its mechanical resonant frequency of 220 kHz. Scattered signals from the detector are routed into a lock-in amplifier, which demodulates the signal with the reference frequency of 220 kHz, the lock-in amplitude of 4th harmonic (880 kHz) is used to produce the near-field image.

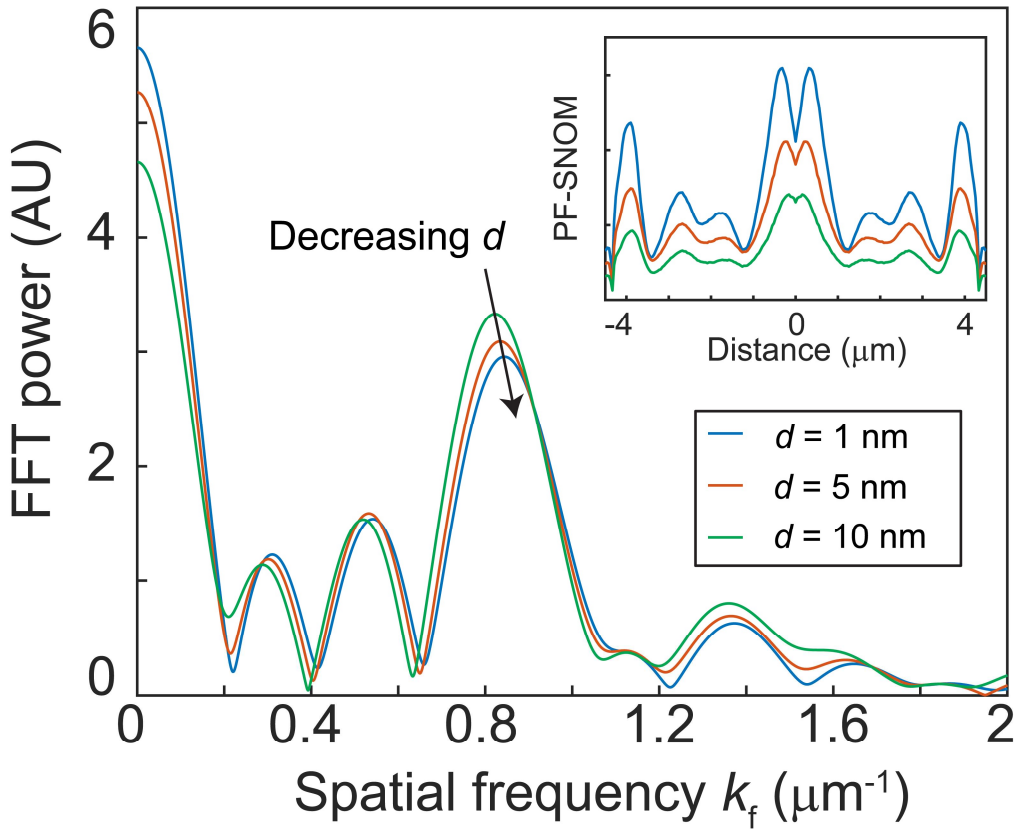

Supplementary Figure S2. Extraction of spatial frequencies. Fringe patterns at $\omega = 1425$ cm^{-1} and $d = 1, 5, 10$ nm are extracted through radial averaging from the center of micro-disk and are displayed in the inset. The same procedure is applied to PF-SNOM images at other ω and d. Resulting fringe patterns are then Fourier Transformed to obtain the spatial frequency of the fringe k_{f}, and to get the polariton momentum q_{p} by $q_{\mathrm{p}} = \pi k_{\mathrm{f}}$.

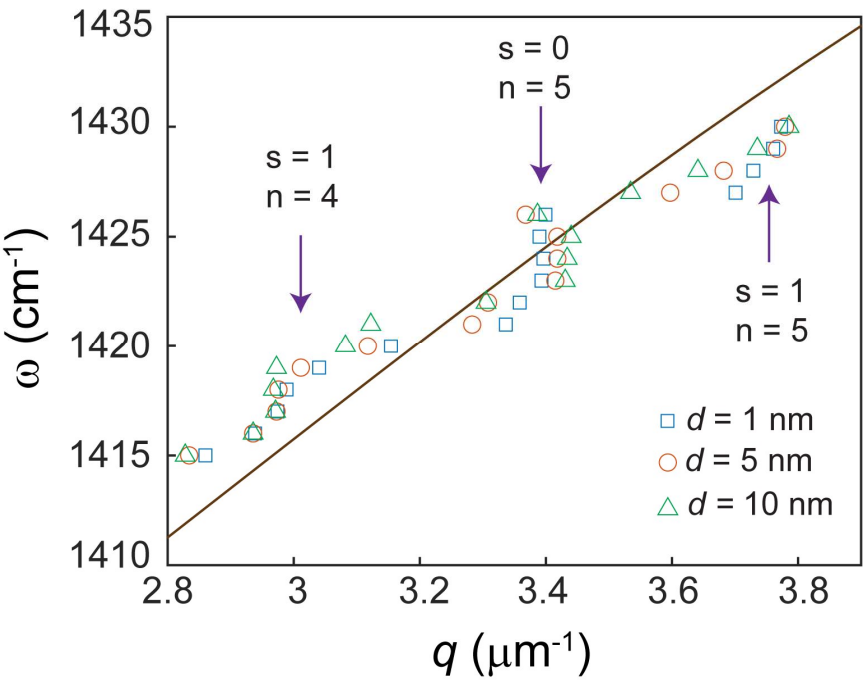

Supplementary Figure S3. Additional PF-SNOM measurement on another *h*-^{11}BN micro-disk. The thickness is 60 nm, and the diameter is 8.9 μm. Experimental data (blue squares, orange circles and green triangles) are overlaid with calculated dispersion relation (brown curve) and resonant conditions (vertical purple arrows, with assigned (s, n) numbers). Similar to Figs. 2e-f in the main text, polariton momentum q_{p} is less dependent of tip-sample distance d at resonant conditions, and changes at different d at non-resonant conditions.

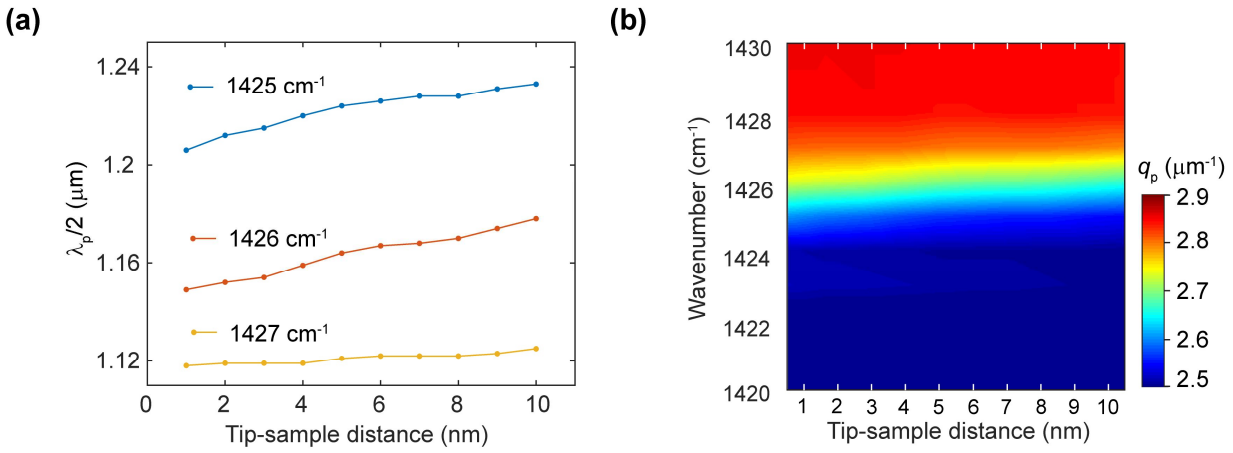

Supplementary Figure S4. Tuning q_{p} by varying tip-sample distance d through PF-SNOM. (a) Under non-resonant conditions such as $\omega = 1425, 1426$ and 1427 cm^{-1}, the wavelength of the fringe pattern λ_{f}, polariton wavelength $\lambda_{\mathrm{p}} = 2\lambda_{\mathrm{f}}$ and polariton momentum $q_{\mathrm{p}} = \frac{2\pi}{\lambda_{\mathrm{p}}}$ can be tuned by changing tip-sample distance d. As this figure shows, as d increases from 1 to 10 nm, λ_{f} increases from 1.206, 1.149, 1.118 to 1.233, 1.178 and 1.125 μm for 1425, 1426 and 1427 cm^{-1}, respectively. (b) A false colormap of polariton momentum q_{p} over $\omega = 1420{-}1430$ cm^{-1} and $d = 1 - 10$ nm. At resonant conditions ($\omega = 1420 - 1422$ and $1428 - 1430$ cm^{-1}), q_{p} does not change with d. On the contrary, at non-resonant conditions ($\omega = 1423 - 1426$ cm^{-1}), q_{p} increases as d increases. These results demonstrate that PF-SNOM is capable of tuning q_{p} under non-resonant conditions and indicate that PF-SNOM can also be used to distinguish whether the system has extrinsic resonance.

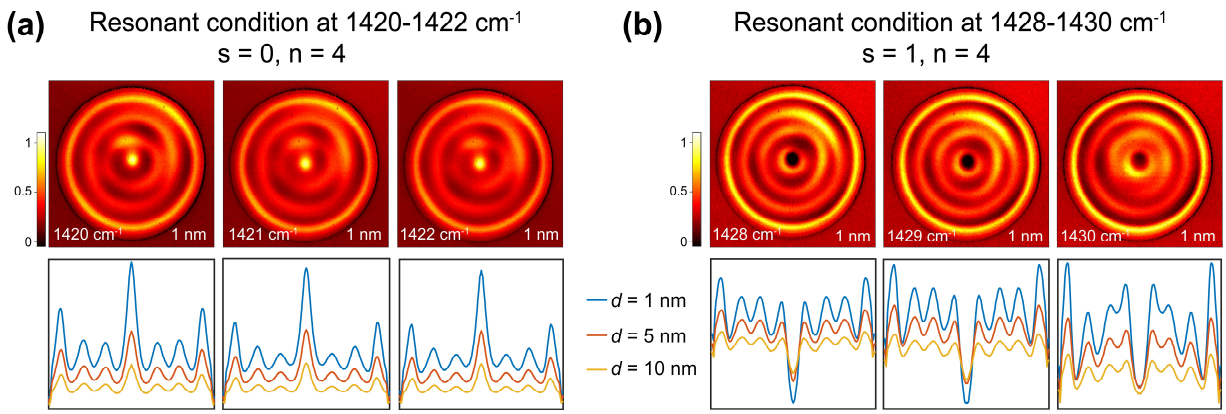

Supplementary Figure S5. Fringe patterns at two adjacent resonant conditions. According to PF-SNOM experimental results and model prediction (**Figs. 3b-c** in the main text), resonant momentum $q_{\mathrm{p}}(s,n)$ increases with the increase of incident frequency ω with alternating s between 0 and 1. In addition, the roundtrip component that we observed in PF-SNOM can be approximated as a square of the Bessel function (**Equation S5**). If we plug $r = 0$ (disk center) into **Equation S5** and omit the anomalous phase shift ϕ, we will get $\rho^2 = J_s^2(0)$, which are constants determined simply by the order s of Bessel function. With $s = 0$ and 1 alternating, we see PF-SNOM signal at the disk center alternating from bright ($s = 0$, $J_0^2(0)$ is local maximum) to dark ($s = 1$, $J_1^2(0)$ is local minimum).

References

1. M. Tamagnone, A. Ambrosio, K. Chaudhary, L. A. Jauregui, P. Kim, W. L. Wilson and F. Capasso, *Science Advances*, 2018, **4**, eaat7189.
2. A. J. Giles, S. Dai, O. J. Glembocki, A. V. Kretinin, Z. Sun, C. T. Ellis, J. G. Tischler, T. Taniguchi, K. Watanabe and M. M. Fogler, *Nano letters*, 2016, **16**, 3858-3865.
3. A. Y. Nikitin, T. Low and L. Martin-Moreno, *Physical Review B*, 2014, **90**, 041407.